JAERI-M
5385

# FIRST REPORT ON THE JAERI TOKAMAK EXPERIMENTS

September 1973

Satoshi ITOH, Noboru FUJISAWA, Akimasa FUNAHASHI, Shunsuke KUNIEDA, Tatsuoki TAKEDA, Tohru MATOBA, Satoshi KASAI, Tohru SUGAWARA*, Kazuo TOI, Norio SUZUKI, Masaki MAENO, Kenji INOUE, Mitsuru OHTA, Shinzaburo MATSUDA, Tokumichi OHGA, Takashi ARAI, Kenji YOKOKURA and Sigeru MORI

日本原子力研究所
Japan Atomic Energy Research Institute

JAERI-M 5385

# First Report on the JAERI Tokamak Experiments

S. Itoh, N. Fujisawa, A. Funahashi, S. Kunieda, T. Takeda, T. Matoba, S. Kasai, T. Sugawara*, K. Toi, N. Suzuki, M. Maeno, K. Inoue, M. Ohta, S. Matsuda, T. Ohga, T. Arai, K. Yokokura, and S. Mori

Thermonuclear Fusion Laboratory, Tokai, JAERI

(Received August 14, 1973)

The experimental results so far obtained with JAERI tokamak JFT-2 are described. The maximum plasma current is 175 kA, the density is $1.4 \times 10^{13}$ $cm^{-3}$, the conductivity electron temperature is 780 eV, the ion temperature is 210 eV, and the energy confinement time is 25 msec. The confinement time is in agreement with the scaling law obtained empirically with the other tokamaks.

---

* On leave from Research and Development Center, Tokyo Shibaura Electric Co., Ltd., Kawasaki.

# 原研トカマク実験の初報

日本原子力研究所東海研究所核融合研究室

伊藤　智之，藤沢　　登，船橋　昭昌，国枝　俊介，竹田　辰興，
的場　　徹，河西　　敏，菅原　亨*，東井　和夫，鈴木　紀男，
前野　勝樹，井上　堅司，太田　　充，松田慎三郎，大賀　徳道，
新井　　貫，横倉　賢治，森　　茂

（１９７３年８月１４日受理）

原研トカマク装置（ＪＦＴ－２）による実験結果の第１報である。ＪＦＴ－２でこれまでにえられた主な結果は次のとおりである。最大プラズマ電流　１７５kA，密度　$1.4\times10^{13}\ cm^{-3}$，電気伝導度からもとめた電子温度　７８０eV，イオン温度　２１０eV，エネルギー閉じ込め時間　２５msec　である。この閉じ込め時間は諸外国のトカマク実験でえられた比例法則と一致する。

---

＊　外来研究員（東芝，総合研究所）

目　次　な　し

## I. Introduction

The construction of the JAERI tokamak marked as JFT-2 has been finished in April, 1972. After the preliminary experiments for about a month, the measurements of the uniformity of the various magnetic fields and the improvement of the vacuum systems, especially the cleaning of the inner surface of the vacuum chamber have been carried out for six months.

After about 4000 high current discharges of 50 to 100 kA, the low voltage of about 0.4 V and the high current of 175 kA have been attained. The effect of the high current discharge cleaning is reported in the separate paper[1].

This paper reports the experimental results obtained during the period from November, 1972 to March, 1973.

The measuring instruments are 4 mm microwave interferometer, the charge exchanged neutral particle energy analyzer and the diamagnetic probes. The fundamental quantities of the loop voltage, the total plasma current and the displacement of the plasma column are measured in the usual way using the various coils.

The main results are the following. The peak conductivity electron temperature (Z=1) is 780 eV, the peak electron temperature obtained by the diamagnetic measurement is 1040 eV, the ion temperature is 210 eV, the electron density is $1.4 \times 10^{13}$ $cm^{-3}$ and the energy confinement time is about 25 msec. The ion temperature and the energy confinement time satisfy the scaling laws which are obtained in the experiments of the T-3 and ST tokamaks.

## II. Dimensions and experimental conditions

The dimensions are shown in Tab. 1, and Figs.1 and 2. The axis of the fan-shaped toroidal field coils is shifted outwards by 10 cm from the aluminum shell axis in order to minimize the non-uniformity of the field at the outer surface of the plasma. The distance between the plasma periphery and the wall is fairly larger than other tokamak devices. This is advantageous in the point of view of the impurities released from the wall by plasma impacts.

The experimental conditions are listed in Tab.2. At first the optimum operating conditions are searched with changing the filling pressure, the charging voltage of the condenser banks for Ohmic heating and the vertical magnetic field. The condition of the case 2, which is mentioned in the

following section, is found to be optimum concerning the conductivity temperature and stable loop voltage waveform. Then the plasma quantities such as the temperature, the energy confinement time and so on have mainly been measured for the case 2.

## III. The survey of the optimum operating condition

The optimum operating condition has been studied with changing the filling pressure, the charging voltage of the condenser banks for Ohmic heating and the vertical magnetic field. The condenser banks consist of the two kinds of banks. One is the 20 kV, 400 $\mu$F bank (the first bank) and the other is the 5 kV, 10400 $\mu$F bank (the second bank). These banks are fired in sequence.

The effect of the DC vertical magnetic field ($B_{VD}$) on the waveforms is shown in Fig.3. The maximum current ($I_p$) is about 140 kA and the loop voltage ($V_{loop}$) is about 0.5 V. The longest duration time of the current is obtained at $B_{VD} \simeq 133$ G. The effect of the pulsed vertical field ($B_{VP}$) is shown in Fig.4. The waveforms of the plasma current and the loop voltage resemble Fig.3, and the longest duration is obtained at $B_{VP} \simeq 120$ G.

The dependence of the waveforms on the charging voltage of the banks can be seen by comparing Fig.4 with Fig.5. In the case of the low voltage, the large amplitude instability appears on the loop voltage at the plasma current corresponding to the integral value of the safety factor q at the limiter.

The effect of the voltage of the second bank is shown in Fig.6. In the case of higher voltage the plasma current increases to 175 kA, which corresponds to $q = 2$, and then decreases gradually to the current corresponding to $q = 3$. From this value the current decreases rapidly. At these values of q the large amplitude instability appears on the loop voltage. In the case of the lower charging voltage, however, the waveform is comparatively smooth, and resembles that of Fig.4.

The waveforms at the higher and lower filling pressures are shown in Fig.7. In these cases the positive spike oscillations appear on the loop voltage.

The various quantities obtained from the above-shown waveforms are compared in Tab.3. From the table the case 2 has been concluded to be the optimum experimental condition. Hereafter the data for the case 2 are mainly discussed.

## IV. The shift of the plasma column

The displacements of the plasma current axis from the shell axis are measured by the magnetic probes. The horizontal and vertical displacements during the discharge are shown in Figs.8 and 9, respectively. The former is about 2 cm inwards, and almost constant during a discharge. In the initial phase corresponding to the skin time of the shell, the latter is about 1.5 cm upwards due to the small error field of 10 G by the toroidal magnetic coils, and increases gradually in course of a discharge.

The gradual increment of the latter is due to the diffusion of the poloidal field by the plasma current through the shell. For the case of the former the poloidal field diffuses also through the shell, but the vertical field by the leakage magnetic field from the iron core penetrates through the shell with the same skin time as that of the diffusion, and compensates the reduction of the effect of the shell. Thus the horizontal displacement is kept constant during a discharge.

## V. The measurements of the plasma quantities

In this section the various measured quantities are shown, and some discussions are given.

### 1. The plasma density

The plasma density are measured by the 4 mm microwave interferometer. The horn is moved horizontally in the interval of 6 cm from the point looking vertically on the shell center in order to measure the density profile. The lenses of the center and two lenses adjacent to them, however, became opaque by sputtering of the limiter. Then the density profile and the density of the center are estimated from the averaged values measured along other five microwave paths.

The time variation of the density averaged over the microwave path is shown in Fig.10 with the corresponding current waveform. Usually the density profile can be obtained by the Abel transformation. But in the present case the Abel transformation may involve the large error due to the deficiency of the data in the central region. Therefore the density profile is conjectured by comparing the experimentally obtained phase shift with those obtained for assumed density profile as in Fig.11. The dots show the density averaged over the microwave path by assuming that the plasma fills the region

in the liner. The curves are calculated by assuming the density profiles and the center densities as shown in the figure. It is suggested that the density profile of $n(r) = 1.4 \times 10^{13} \times \{1-(r/a_{lin})^4\}$ agrees with the experimental result.

The time variation of the center density estimated by the above-mentioned method is shown in Fig.12. This shows that the density is nearly constant except initial phase.

2. The ion temperature

The ion temperature is measured by the charge exchanged neutral particle analyzer. The details of the analyzer are reported in references (2) and (3).

The typical results detected on the median plane in the condition of case 2 are shown in Fig.13. It is deduced from the figure that the ions are constituted of the high energy component of 210 eV ("hot") and the low energy component of 80 eV ("cold"). The detected total flux of neutral particles for the hot ions acounts for $2 \times 10^8$ msec$^{-1}$. Then, for the hot ions $V_h \langle n_{nh} \cdot n_{ih} \rangle \simeq 2 \times 10^{21}$ cm$^{-3}$ is obtained by assuming $\langle n_{ih} \rangle \simeq 10^{13}$ cm$^{-3}$, where $V_h$ is the effective volume looked into from the analyzer, $n_{nh}$ is the neutral particle density existing in the hot ion region, $n_{ih}$ is the hot ion density and the brackets mean the average over the occupied space. Using this value and the figure $V_c \langle n_{nc} \cdot n_{ic} \rangle \simeq 6.24 \times 10^{21}$ cm$^{-3}$ is calculated for the cold ions, where the suffix c means the cold component.

The radial profile of the ion temperature is roughly estimated as follows. The hot and cold ions are generally expected to occupy the central and outer regions of the plasma column, respectively. Then at first the ion temperature profile is assumed to be rectangular as shown in Fig.14. The actual profile, however, is smooth function of r, for example, $T_{io}\{1-(r/a)^m\}$, where a is the minor plasma radius. By assuming that the averaged ion temperature of the rectangular profile is equal to the averaged temperature of the profile of the form $\{1-(r/a)^m\}$, and using the above-obtained values and the plasma density profile shown in the foregoing paragraph, the following relations are deduced.

$$\frac{r_c}{a} = \frac{1}{0.62}\left(\frac{m}{m+2} - 0.38\right) \quad , \tag{1}$$

$$\alpha \equiv \frac{\langle n_{nh} \rangle}{\langle n_{nc} \rangle} \simeq \frac{1}{3.12}\left(\frac{a}{r_c} - 1\right) \quad . \tag{2}$$

The relations are drawn in Fig.15. The neutral density of the central region is expected to be much smaller than that of the outer region[4] and $\alpha$ is expected to be 0.1~0.2. Then m = 5.5~3 and $r_c/a = 0.75 \sim 0.6$ are obtained. Thus the hot ions seem to occupy the rather large region and to be main components of ions.

The scaling law for the ion temperature obtained empirically in other tokamaks is shown in Fig.16 with the results of JFT-2.

## 3. The electron temperature

In the present experiments the Thomson scattering method has not been used. The electron temperature is calculated from the plasma conductivity using the Spitzer's equation. The averaged temperature $(\overline{T_e+T_i})$ is also measured using the diamagnetic coils.

The inner inductance, which is used to deduce the conductivity temperature, is calculated from the measured displacement as in Fig.17. The poloidal beta $\beta_p$ is also shown in Fig.18.

The time variations of the conductivity electron temperature* and the averaged temperature are shown in Fig.19 with the peak ion temperatures. In this figure it is assumed that the temperature is flat over the whole plasma region (a = 23 cm), Z = 1 and the averaged density is $9.3 \times 10^{12}$ cm$^{-3}$. If the radial profile of the electron temperature is assumed to be $T_{eo}\{1-(r/a)^2\}$ (figure 17 suggests that the profile is much sharper), the peak conductivity electron temperature is 780 eV at t = 90 msec. As the averaged ion temperature is 140 eV for m = 4, the averaged electron temperature deduced from the diamagnetic measurement is obtained roughly to be 520 eV at t = 90 msec. Then the peak electron temperature is about 1080 eV. By comparing this value with the conductivity electron temperature, the effective charge $(Z_{eff})$ is deduced as 1.4. This value suggests that the containment of impurities in the JFT-2 plasma are very little.

## 4. X-ray

The preliminary measurements of x-ray radiation have been carried out in order to investigate the runaway electron.

Toroidal distribution of the x-ray dose is measured with pocket dosimeter

*This value is somewhat different from that of the paper[5] submitted to the 3rd International Symposium on the Toroidal Confinement. The difference is due to the contribution from the time derivative of the plasma inductance which was neglected in the paper.

outside the toroidal coils. Results are shown in Fig.20. It is concluded that the hard x-ray radiation occurs by impact of runaway electrons to the limiter. The angular distribution also indicates that the energy of runaway electrons exceeds several hundreds keV.

The time dependence of production of the hard x-ray is measured with a NaI scintillator and a photomultiplier. In the optimum conditions in which a plasma is comparatively stable, the hard x-ray is produced continuously and the energy of the hard x-ray increases with time.

The energy spectrum of the hard x-ray is measured in the condition of case 2. The result is shown in Fig.21. It is shown that the energy of runaway electrons increases with time and that the number of them also increases with time. These characteristics indicate that the runaway electrons are maintained long under a stable discharge. More detailed measurements are to be performed with respect to the creation of the runaway electrons and the disappearance of them.

## VI. The energy confinement time

The energy confinement time is deduced using the diamagnetic signal. The time variation of the total input energy, the total plasma energy and the time derivative of the total energy are shown in Fig.22. Here the total energy input ($Q_{in}$) is defined as $Q_{in} = I_p V_{loop} - 0.5(d/dt)[I_p^2\{L_{ext} + (\mu_o R_o/2) l_i\}]$ using Fig.17 and $L_{ext} = \mu_o R_o \ln(b/a)$, where $R_o$ is the major radius of plasma, a is the minor radius of plasma and b is the inner radius of the shell. b must be the distance between the plasma current axis and the loop coil for the measurement of the loop voltage. But it is reasonable that the shell radius is used as b, because the loop coil is set on the inner surface of the shell at the present case.

The energy confinement time $\tau_E = W/(Q_{in} - \dot{W})$ is deduced as in Fig.23 using Fig.22. This shows that the maximum energy confinement time reaches about 25 msec, which is the longest value than that ever obtained in other tokamaks.

The scaling law $\tau_E = (4 \sim 5) \times 10^{-8}\ a^2 (a/R_o)(B_t/q)$ (in Gaussian unit) obtained empirically in T-3 and ST tokamaks is shown in Fig.24 with the present results. The figure shows that the scaling law can be extended to the value of 25 msec and the large plasma radius of 23 cm.

## VII. Summary

The experimental results which have been obtained so far are summarized as the following.

(1) The horizontal displacement of the plasma column is able to be made small and kept constant during the discharge by adjusting the externally applied vertical field. Thus the equilibrium of the plasma is attained.

(2) The vertical displacement increases in the course of the discharge due to the small error field by the toroidal magnetic coils. By compensating the field the displacement could be made small, and the duration of the discharge increased from 0.2 sec to 0.8 sec.

(3) The density profile is rather flat as $n(r) = n_o\{1-(r/a_{lin})^4\}$, and the density on the minor axis is $1.4 \times 10^{13}$ cm$^{-3}$ for the opimum condition of case 2.

(4) The peak ion temperature is 210 eV, and the radial profile is expected to be the form $\{1-(r/a)^{3\sim5.5}\}$.

(5) The peak conductivity electron temperature and the peak electron temperature obtained from the diamagnetic measurement are 780 eV and 1040 eV, respectively. Then the effective charge is $Z_{eff} = 1.4$.

(6) Hard x-ray is emitted by the impact of runaway electrons to the limiter, and the energy of the runaway electrons exceeds several hundreds keV.

(7) The energy confinement time is 25 msec, which agrees with the empirical scaling law obtained by other tokamaks. This means that the scaling law can be extended to the large confinement time of 25 msec and the large plasma radius of 23 cm. Thus the results by JFT-2 is encouraging in designing the large tokamaks aimed at the scientific feasibility experiments.

## Acknowledgement

The authors are very grateful to Dr. S. Yano, the chief of the Ionized Gas Laboratory, and his group for the measurements of the ion temperatures.

## References

1) N.Fujisawa et al.: JAERI-M5369 (July, 1973).
2) S.Yano et al.: JAERI-M5276 (May, 1973).
3) A.Kitamura, K.Takahashi and S.Yano: JAERI-M5275 (May, 1973).
4) E.I.Kuzunetsov and N.D.Vinogradova: Soviet Phys. JETP Letters 8, 34 (1968).
5) S.Itoh et al.: "Tokamak Experiments at JAERI", The Third Intern. Symposium on Toroidal Plasma Confinement, March, 1973, B-4.

Table 1 Dimensions of JFT-2

| | | |
|---|---|---|
| Major Radius | (cm) | 90 |
| Minor Radius | (cm) | |
| Vacuum Chamber (Liner) | | 30 |
| Shell | | 36 |
| Thickness | (cm) | |
| Liner | | 0.06 |
| Shell | | 3 |
| Fixed Limiter | | |
| Radius of L | (cm) | 25 |
| M | | 20 |
| S | | 16.3 |
| Dynamic Limiter | | |
| Minimum Distance | (cm) | 24 |
| Maximum Distance | (cm) | 49 |
| Maximum Speed | (m/sec) | 9 |
| Maximum Toroidal Magnetic Field | (kG) | 10 |
| Maximum Vertical Magnetic Field | (G) | |
| DC | | 200 |
| Pulsed | | -200 |
| Flux of the Iron Core (without Bias) | (V·sec) | 0.58 |

Table 2 Experimental conditions

| | |
|---|---|
| Toroidal Field (kG) | 10 |
| Vertical Field (G) | 40 — 150 |
| Filling Pressure (Torr·$H_2$) | $6\times10^{-5}$ — $6\times10^{-4}$ |
| Charged Energy of the Ohmic Heating Banks (kJ) | 60 — 172 |
| Preheating | |
| Frequency (GHz) | 30 |
| Power (kW) | 1 |
| Duration (ms) | 2 |
| The radius of Limiter (cm) | 25 |
| Maximum Plasma Current (kA) | 175 |

Table 3 Principal plasma parameters for various experimental conditions

| | Experimental Conditions | | | | | Max. Current (kA) | Loop Voltage (V) | Current Duration (ms) | Cond.(*) Temp. (eV) |
|---|---|---|---|---|---|---|---|---|---|
| | Filling Pressure (Torr) | $V_t$ (kV) | $V_2$ (kV) | $B_{VD}$ (G) | $B_{VP}$ (G) | | | | |
| case 1 | $3.0\times10^{-4}$ | 18 | 4.0 | 150 | 120 | 175 | 2.6 | 80 | 110 |
| 2 | $1.6\times10^{-4}$ | 18 | 2.6 | 133 | 120 | 149 | 0.3 | 200 | 450 |
| 3 | $1.6\times10^{-4}$ | 10 | 2.0 | 90 | 70 | 94.5 | 0.6 | 120 | 250 |
| 4 | $3.0\times10^{-4}$ | 18 | 2.6 | 133 | 120 | 149 | 0.8 | >200 | 250 |
| 5 | $6.0\times10^{-4}$ | 18 | 4.0 | 119 | 120 | 131 | 8.0 | 60 | 54 |
| 6 | $6.0\times10^{-5}$ | 18 | 4.0 | 134 | 120 | 135 | 0.3 | 320 | 310 |

(*) R = 90 cm, a = 25 cm, Inductance is neglected.

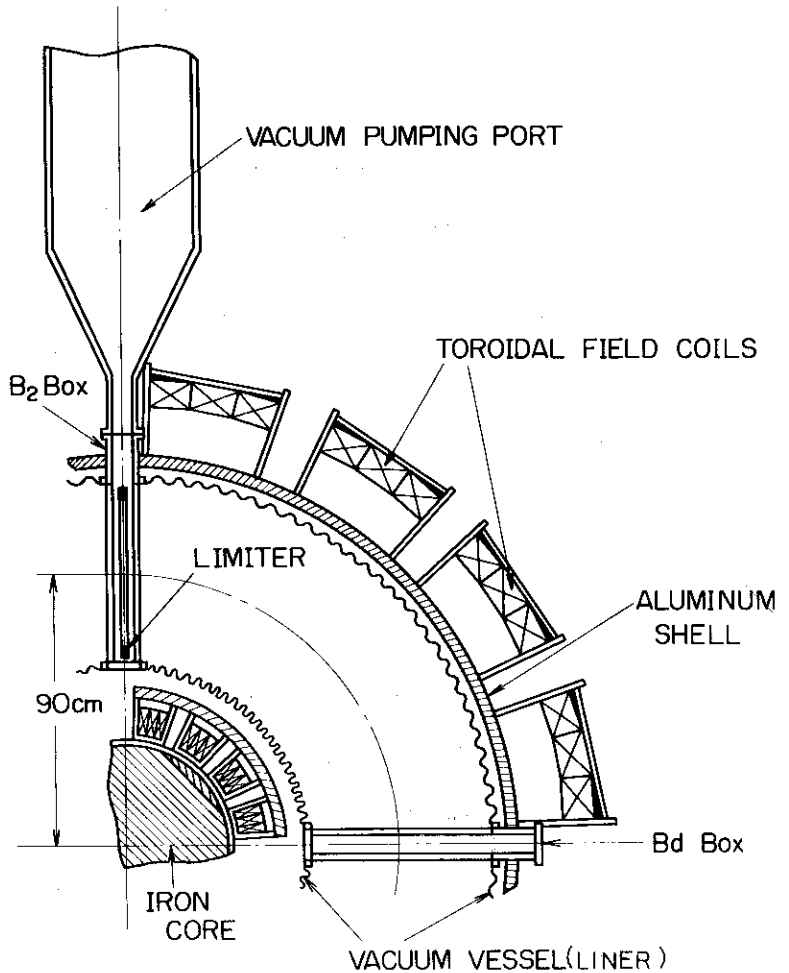


Fig. 1 Plan section of one quadrant of JFT-2

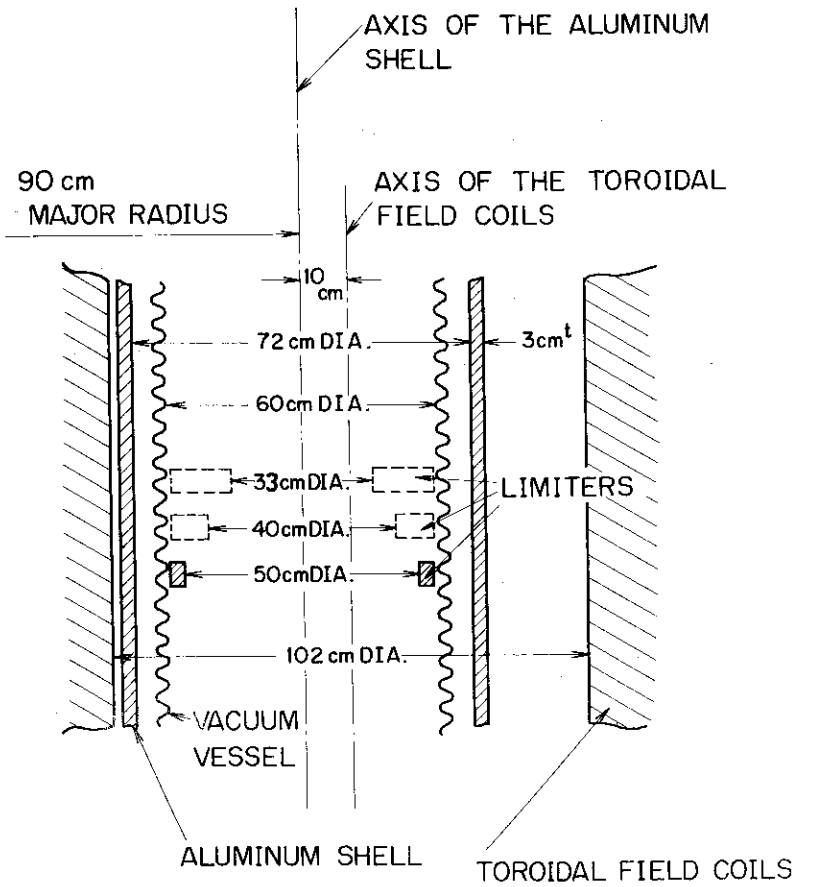


Fig. 2 Minor dimensions for JFT-2

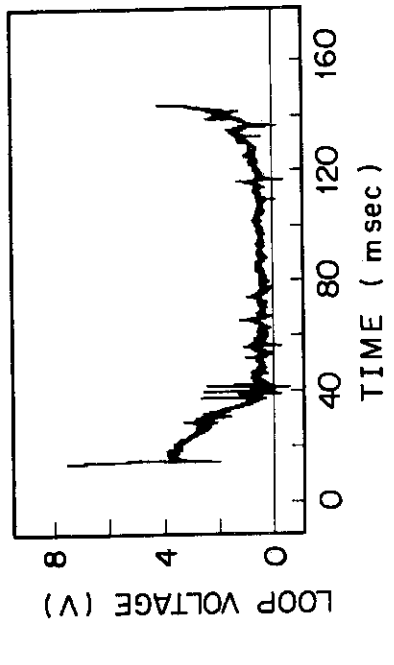


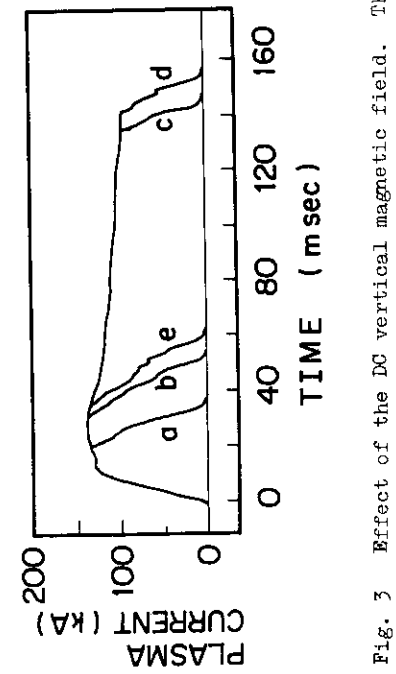


Fig. 3 Effect of the DC vertical magnetic field. The charging voltage of the first bank ($V_1$) is 18 kV, the charging voltage of the second bank ($V_2$) is 2.6 kV, the filling pressure ($P_f$) is $1.6 \times 10^{-4}$ Torr, the magnetic flux density of the pulsed vertical field ($B_{Vp}$) is 120 G. a-the flux density of the DC vertical magnetic field ($B_{VD}$) is 165 G; b-158 G ; c-141 G ; d-133 G; e-126 G. The waveform of the loop voltage corresponds to that of d.

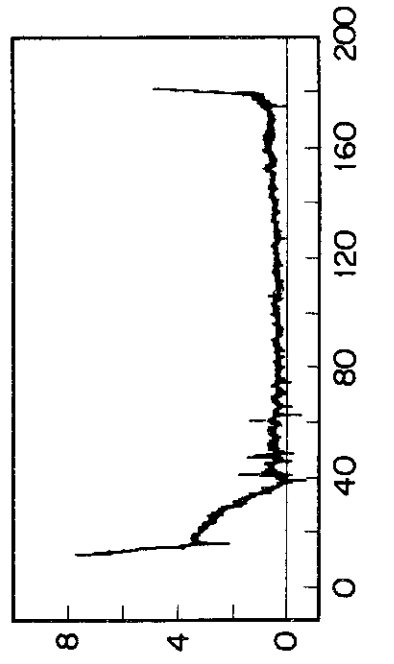


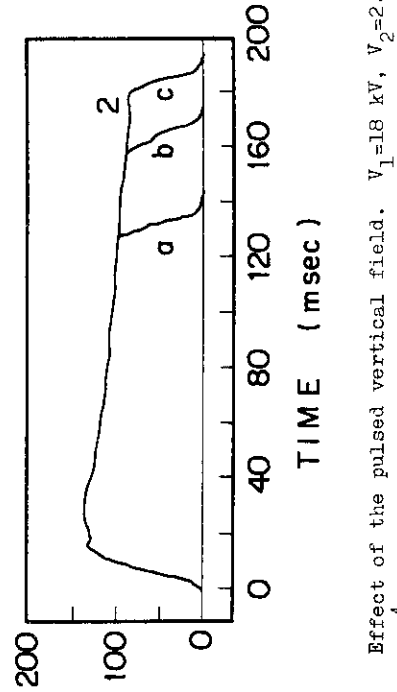


Fig. 4 Effect of the pulsed vertical field. $V_1$=18 kV, $V_2$=2.6 kV, $P_f$=1.6 x $10^{-4}$ Torr and $B_{VD}$=133 G. a-$B_{Vp}$=90 G ; b-110 G ; c-120 G The waveform of the loop voltage corresponds to that of c.

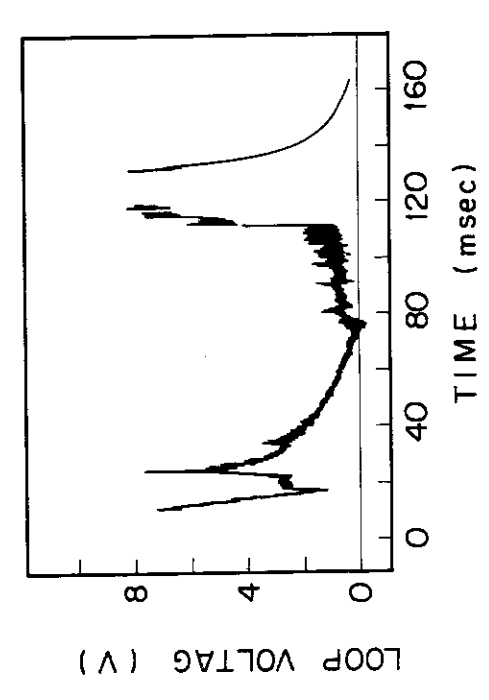


Fig. 5 Waveforms for the low bank voltage. $V_1$=10 kV, $V_2$=2 kV, $P_f$=1.6 x $10^{-4}$ Torr, $B_{VD}$=90 G and $B_{VP}$=70 G.

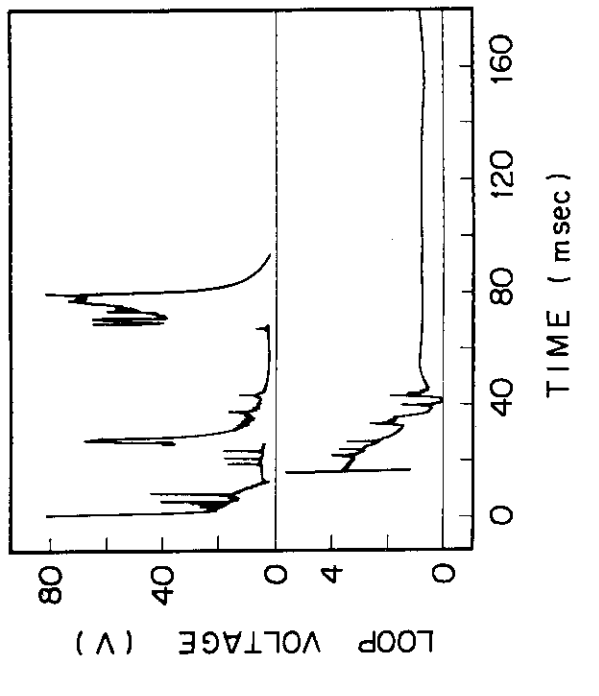


Fig. 6 Effect of the voltage of the second bank. $V_1$=18 kV, $P_f$=3 x $10^{-4}$ Torr and $B_{VP}$=120 G. 1-$V_2$=4 kV, $B_{VD}$=150 G ; 2-$V_2$=2.6 kV, $B_{VD}$=133 G.

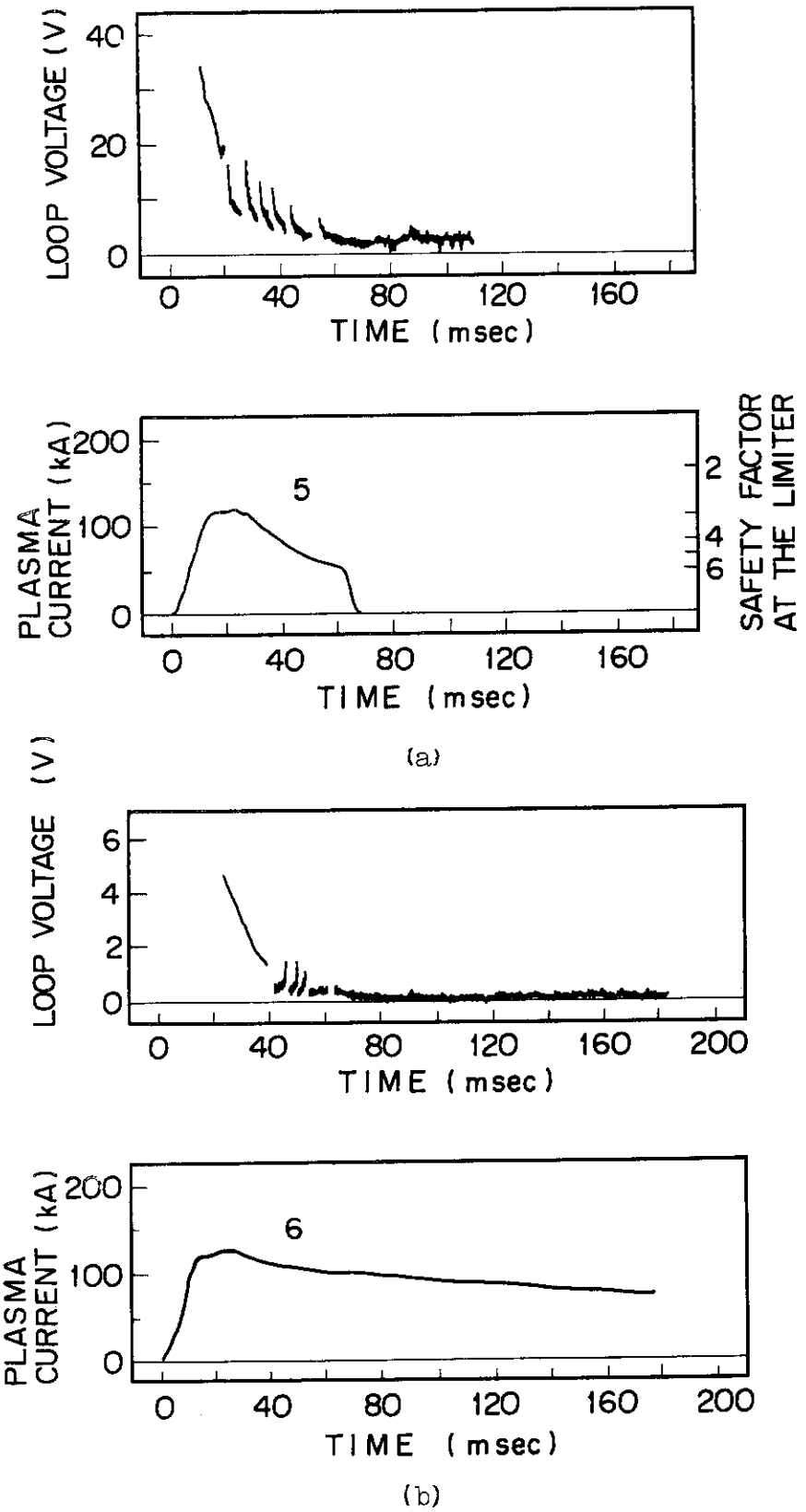


Fig. 7 Waveforms for the higher and lower filling pressures. $V_1$=18 kV, $V_2$=4 kV and $B_{VP}$=120 G. (a)-$P_f$=6 x $10^{-4}$ Torr, $B_{VP}$=119 G; (b)-$P_f$=6 x $10^{-5}$ Torr, $B_{VD}$=134 G.

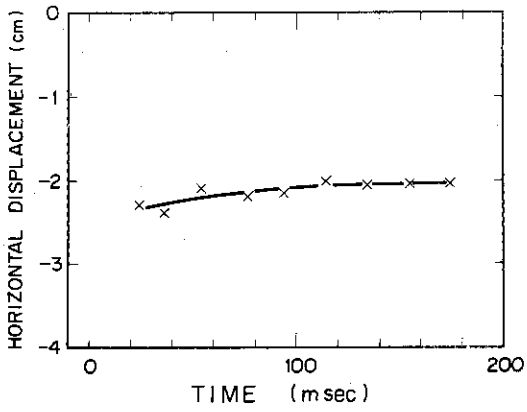


Fig. 8 Horizontal displacement in the condition of case 2.

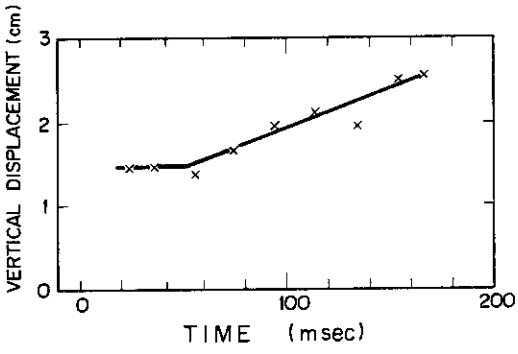


Fig. 9 Vertical displacement in the condition of case 2.

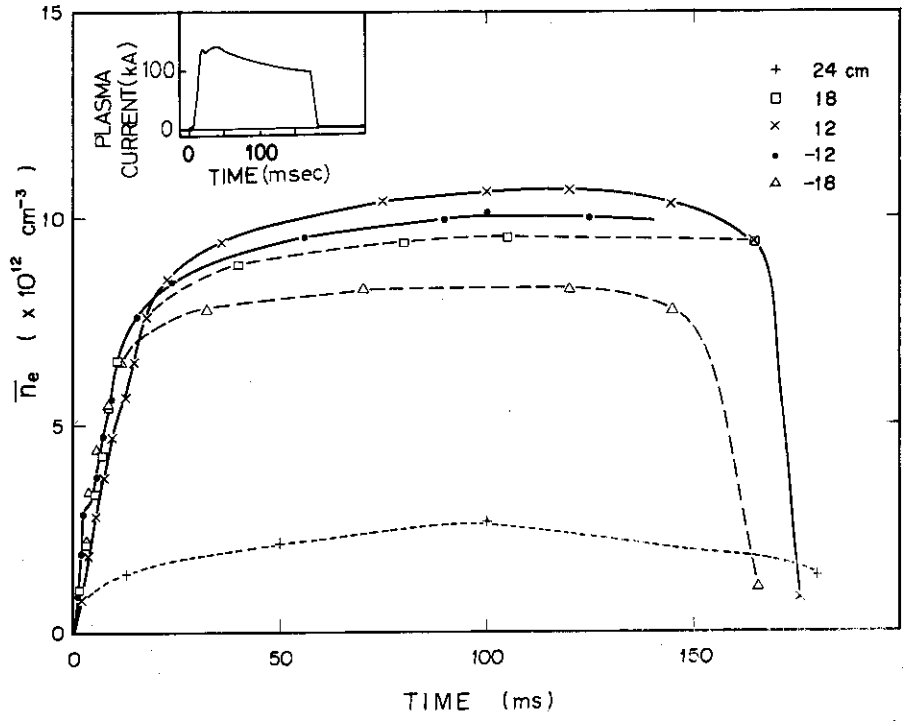


Fig. 10 Time variation of the densities averaged over the microwave paths in the condition of case 2.

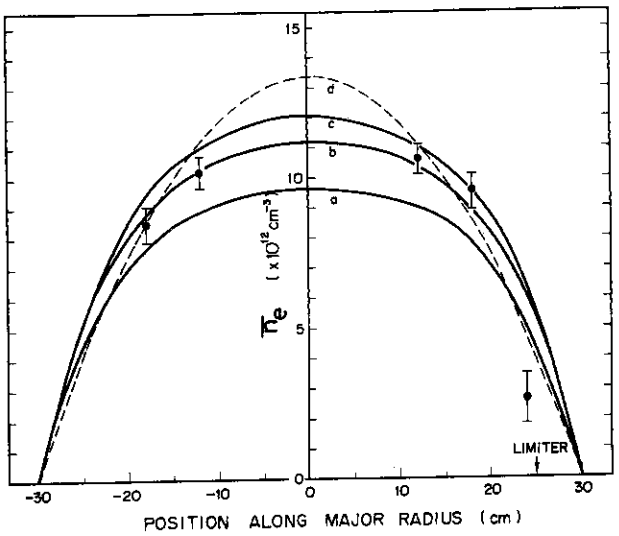


Fig. 11 Comparison between the measured and the calculated densities ($t = 100$ msec). Dots are the measured densities averaged over the microwave paths. Solid and dotted lines are calculated by assuming the density profiles as $a - 1.2 \times 10^{13} \times \{1-(r/a_{lin})^4\}$, $b - 1.4 \times 10^{13} \times \{1-(r/a_{lin})^4\}$, $c - 1.5 \times 10^{13} \times \{1-(r/a_{lin})^4\}$ and $d - 1.4 \times 10^{13} \times \{1-(r/a_{lin})^2\}$, where $a_{lin}$ is the radius of the liner.

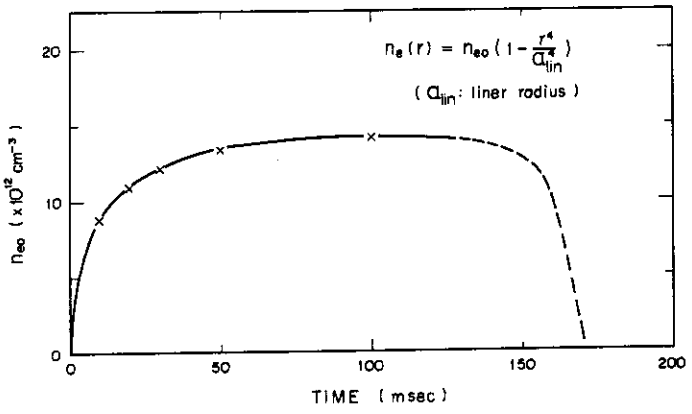


Fig. 12 Time variation of the density on a minor axis.

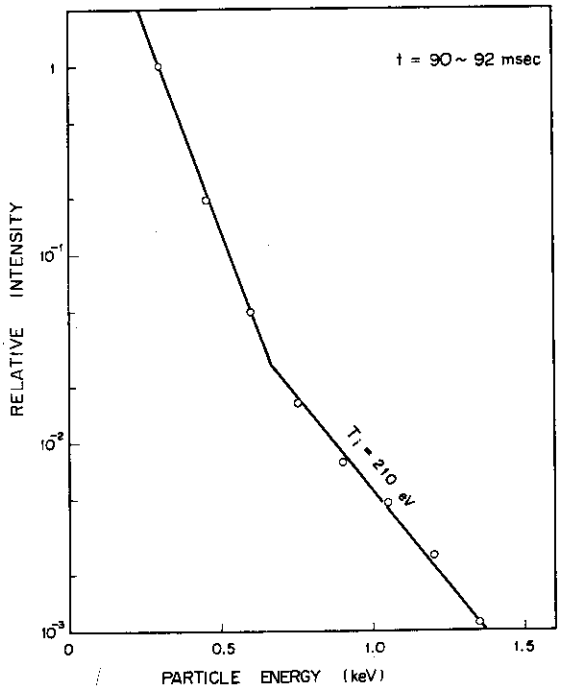


Fig. 13 Total counts of the charge exchanged neutral particles vs particle energy in the condition of case 2 ($t = 90$ msec).

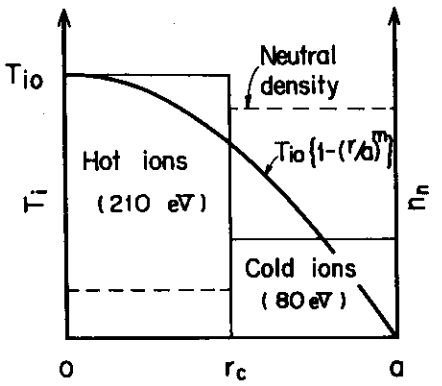


Fig. 14 Model of the ion temperature profile.

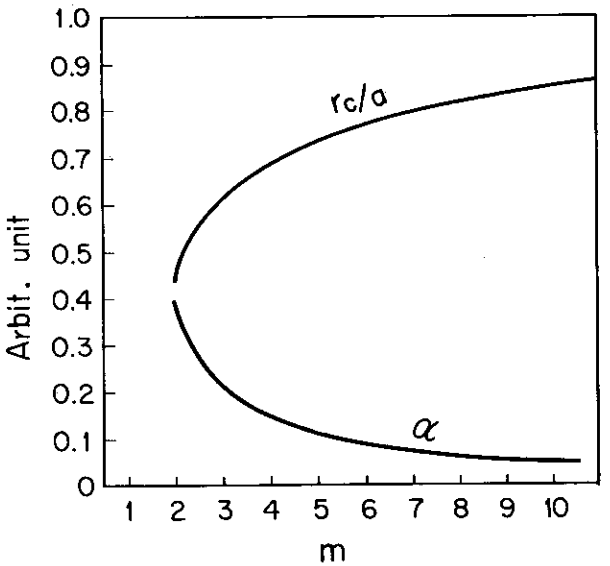


Fig. 15 Drawing of Eqs. (1) and (2).

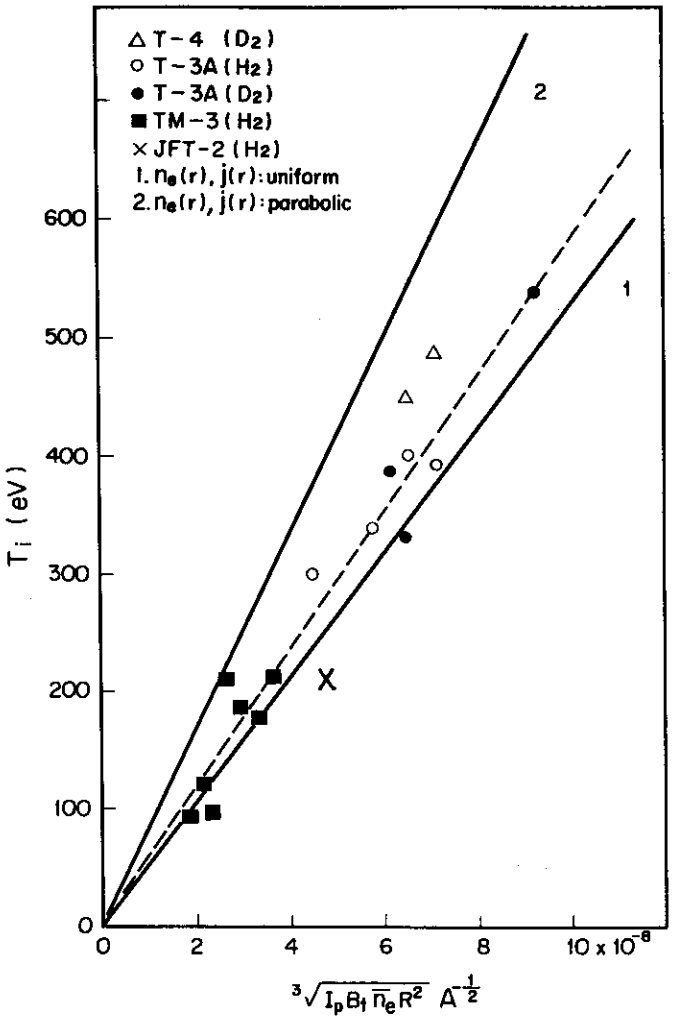


Fig. 16 Scaling law of the ion temperature.

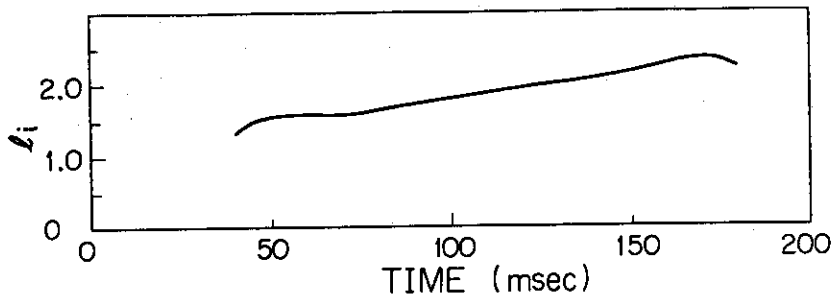


Fig. 17 Time variation of the inner inductance of the plasma in the condition of case 2.

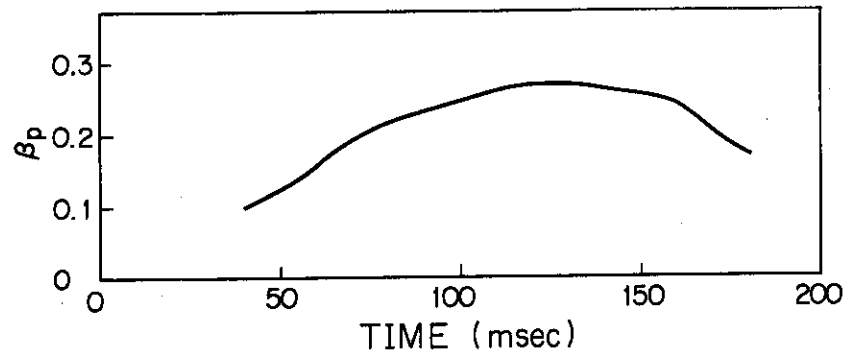


Fig. 18 Time variation of the poloidal beta in the condition of case 2.

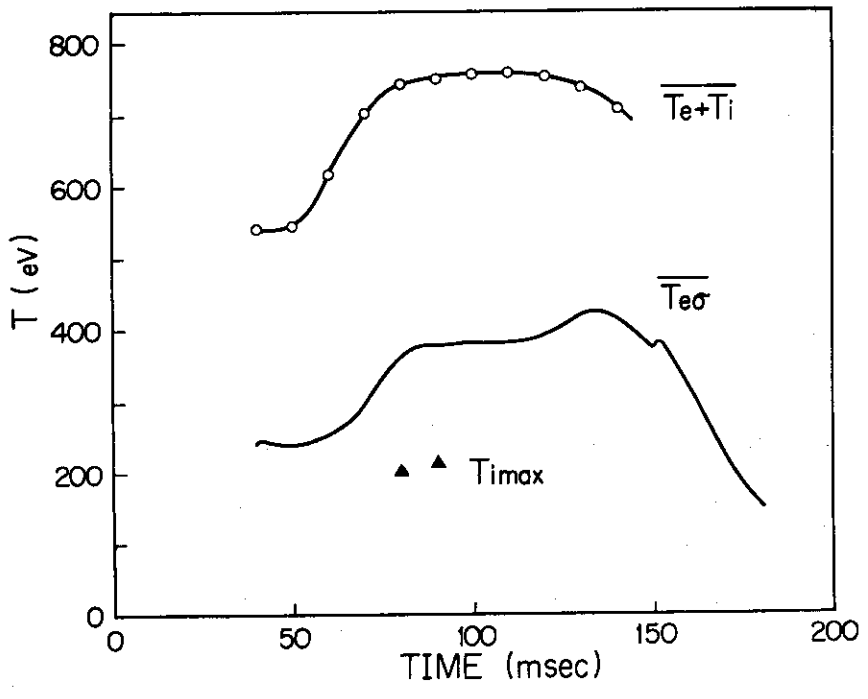


Fig. 19 Time variations of the averaged conductivity electron temperature and the averaged plasma temperature by diamagnetic measurements. The flat radial profile of the temperatures, the density profile of $n(r)=1.4 \times 10^{13} \times \{1-(r/a_{lin})^4\}$ and Z=1 are assumed.

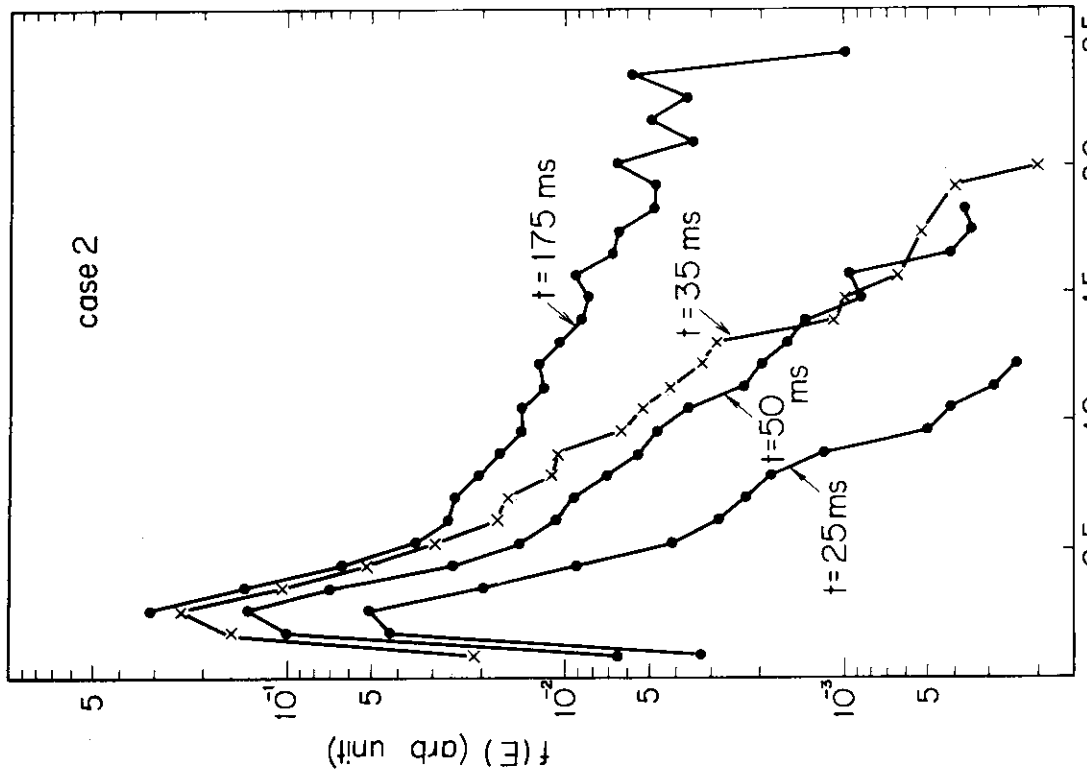


Fig. 21 Energy spectrum of hard x-ray in the condition of case 2. The correction to the slit of Pb and to the detecting efficiency of NaI is performed.

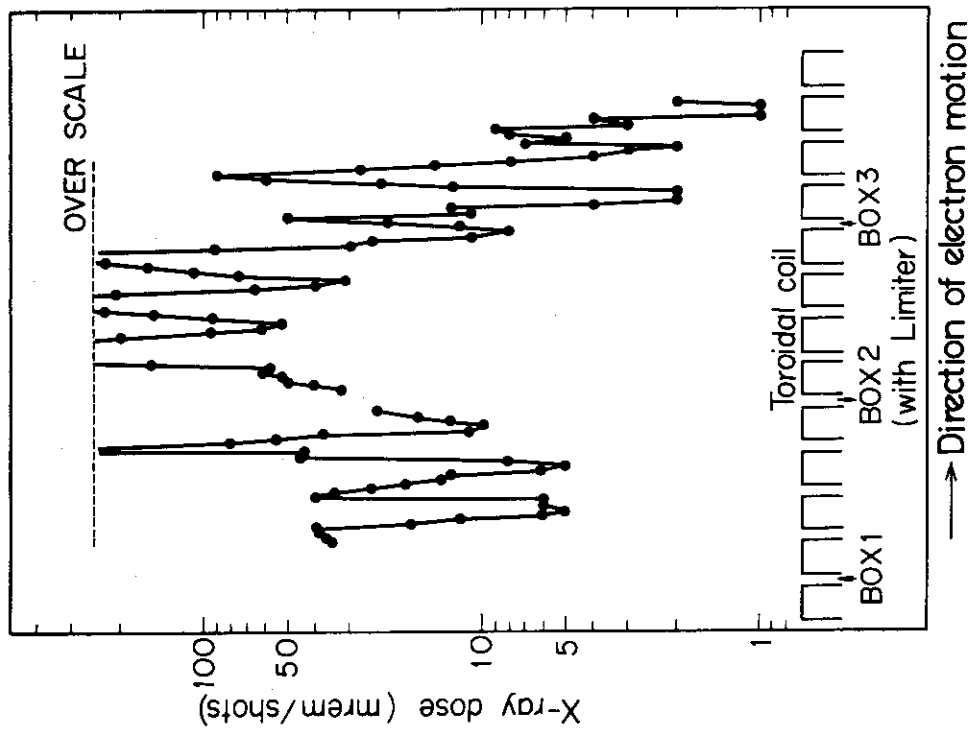


Fig. 20 Toroidal distribution of x-ray dose measured with pocket dosimeter at R=170 cm on the median plane (outside the toroidal coils). The dose behind the toroidal coils is one order smaller than that in the face of the limiter.

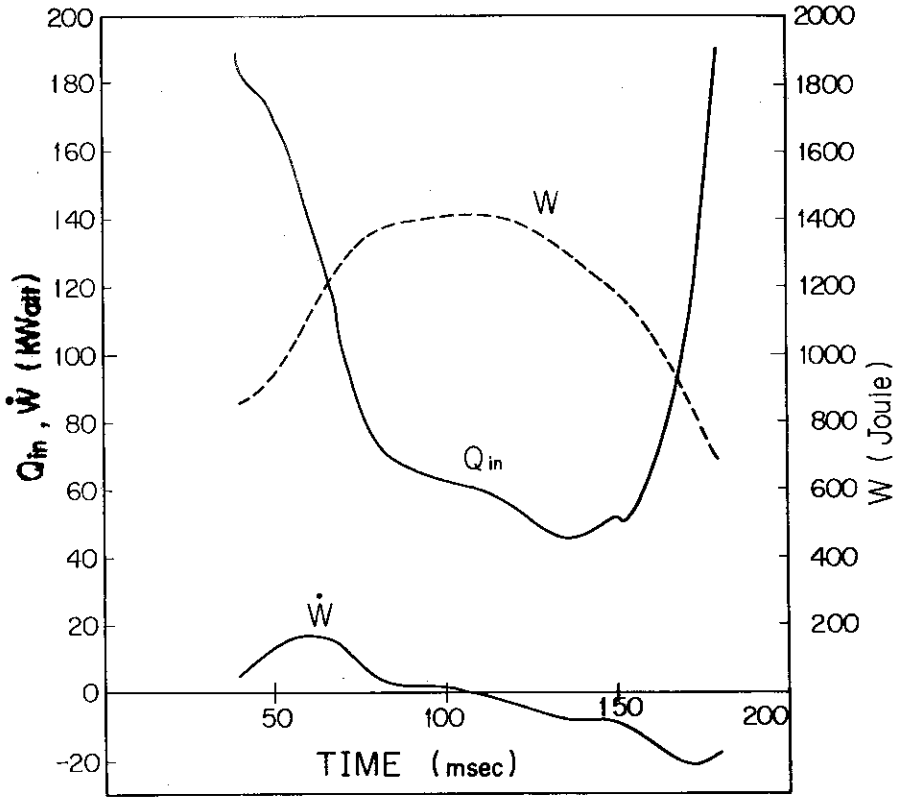


Fig. 22 Time variations of the total input energy ($Q_{in}$), the total plasma energy (W) and the time derivative of the plasma energy ($\dot{W}$). The discharge condition is case 2; $Q_{in}$ is defined as $I_p[V_{loop}-(1/2I_p)\{(d/dt)(LI_p^2)\}]$, where $L=L_{ext}+(\mu_o R_o/2)l_i$. The total plasma energy is measured by diamagnetic coils.

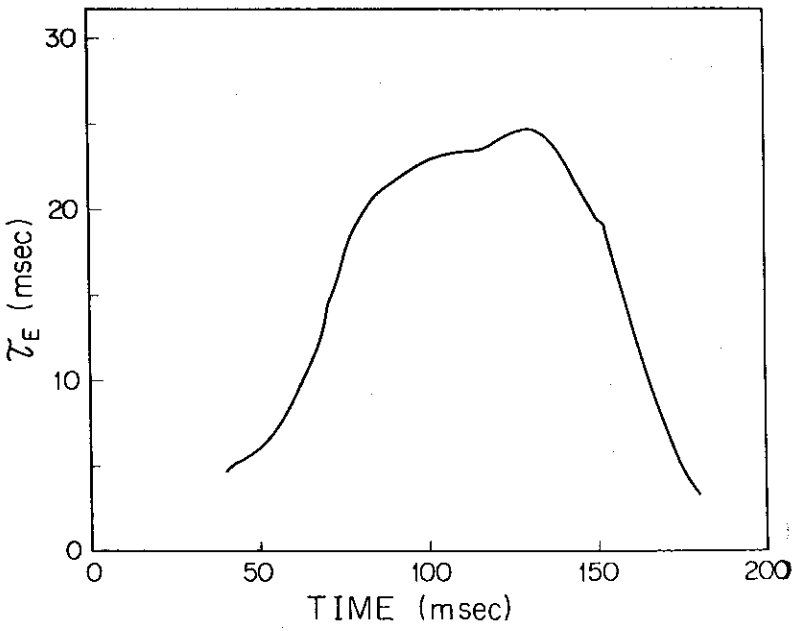


Fig. 23 Time variation of the energy confinement time defined as $\tau_E=W/(Q_{in}-\dot{W})$ in the condition of case 2.

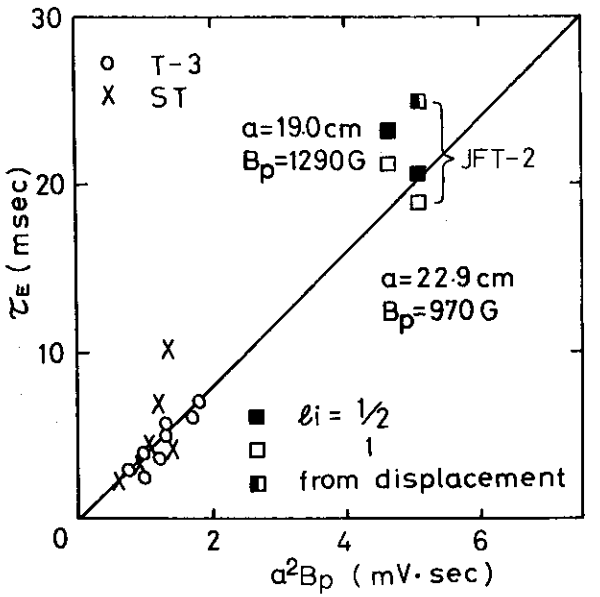


Fig. 24 Scaling law of the energy confinement time.